

Glacial Ice and Offshore Structure Impacts under Wave and Current Excitation

Wenjun Lu^{1,2}, Jørgen Amdahl³

¹ ArcISo AS (Trondheim, Norway)

² Centre of Sustainable Arctic Marine and Coastal Technology (NTNU, Trondheim, Norway)

³ Department of Marine Technology (NTNU, Trondheim, Norway)

ABSTRACT

Bergy bits and growlers (i.e., glacial ice features with a waterline diameter < 15 m) travelling with waves can pose great threats to offshore structure and ships operating in the high North. It is generally more difficult to detect and monitor these small ice features and apply concurrent ice management operations. Therefore, it is important to study the consequence and conduct corresponding damage assessment of potential impacts with such glacial ice features. Before conducting damage assessment, it is critical to know the potential impact location, probability of impact and the associated impact velocities for given environmental conditions (i.e., wave and current). This paper offers a method to conduct time domain coupled motion simulations of the ice feature and the offshore structure given their respective frequency domain properties (i.e., Response Amplitude Spectrums, RAOs). When their coupled motions are simulated in the time domain, we can explicitly sample the outcome of potential impact between these two bodies. For each impact scenario, the correlated impact velocity and the vertical location of impact are available. The sampled impact information enables us to quantify the ice feature's impact probability and impact velocity at different locations of the offshore structure, thereby offering us more accurate damage assessment. This method is proved to be rather efficient and can be used in post-processing of hydrodynamic analysis when dealing with collision studies of multiple bodies. The method also shows that the current velocity plays an important role, as lower current velocity tends to increase the impact probabilities at higher locations of the structure.

KEY WORDS: Glacial ice, Impact, Wave induced motions, Offshore structure

INTRODUCTION

The Petroleum Safety Authority Norway (Norway) established a series of projects to study the structural safety in the Northern areas (i.e., Northern Barents Sea). Within these projects, great interests have been allocated to the impacts between a small glacial ice features with a common offshore structure (e.g., semi-submersibles) in the Barents Sea. With regard to the small ice feature, bergy bits and growlers with a waterline diameter smaller than 15 m are of particular

interests since they are generally more difficult to detect, monitor and manage due to their limited size. Ekeberg et al. (2018) in their report (i.e., ST5), performed extensive studies ranging from bodies' motion in waves, to impact energy analysis, and to structural damage assessment. The basics of the problem are sketched in Figure 1, i.e., an ellipsoidal glacial ice feature with a long axis of 15 m, under the influences of wave (and current) is in collision course with a structure (represented by a cube). The first important question is what the impact locations and velocities are, given certain environmental conditions. In the previous study (Ekeberg et al., 2018), each body's (i.e., glacial ice and the structure) Response Amplitude Spectrums (RAOs) were calculated. Depending on the relative positions between the ice feature and the structure in the frequency domain, an estimation of the impact height range (see Figure 1b) and impact velocity range were obtained.

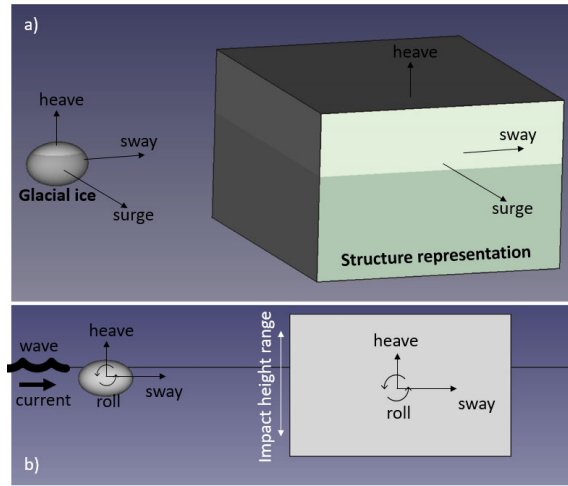


Figure 1. Sketch of the problem together with coordinate definitions.

However, the previous work were mainly performed in the frequency domain (or for a handful cases, a single body's time-domain nonlinear analysis was converted into the frequency domain for analysis). In its totality, the possibility of impact at different heights and the impact's associated impact velocity are not known. This paper is therefore focusing on presenting a method to establish the correlation between the impact location and its associated impact velocity. This requires the simulation of the two bodies' coupled motion (i.e., the glacial ice and the structure) explicitly. This directly leads to coupled solutions of the potential impact height and impact velocity's histories, from which, impact events can be sampled to construct their statistical distribution.

METHODS

To establish the correlation between the impact height and its associated impact velocity, this paper adopts the existing RAOs for each body of the two impacting bodies and simulates their motion in the time domain in a given sea state. For exemplifying purpose, we choose the same ellipsoidal and semi-submersible structure (e.g., see Figure 2) analysed in previous studies. With known relative motions of the two body, the method by Fylling (1994) is utilized to sample impact events (with both impact location and velocity). This method is rather efficient in constructing and sampling impact events. With a large amount of sampled impact events, the distribution of and correlation between impact height and impact velocity can be obtained.

Assumptions and simplifications

This paper mainly focuses on the impact height and its associated impact velocity. The stated three dimensional problem in Figure 1 is thus reduced to a two dimensional problem in Figure 2, in which, only sway, heave and roll motions are considered for each of the two bodies. Impacts at different locations around the structure in the surge direction (see Figure 1) are not considered. Moreover, this method largely depends on the RAOs functions to calculate the wave induced motions. The available RAOs were calculated by WADAM analysis, in which, a constant water plane area has been assumed. This might lead to unrealistically large vertical reaction force particularly for the ellipsoidal glacial ice feature considered in this paper. As this glacial ice feature, in certain wave conditions might be totally submerged. This effect is not considered in the followed-up calculations. Nevertheless, this will not hamper the essence of the proposed method in this paper. This is to day, updated methods considering the nonlinear effects (e.g., submergence) can be incorporated into this method.

Relative motion in a single wave component

Before the method for a complete sea state are presented, let us look at a simpler case, i.e., motions of a body in a regular wave. For a single wave component with frequency ω , wave number $k = 2\pi / \lambda$, wave length $\lambda = 1.56(2\pi / \omega)^2$ and a random phase angle ϕ , its vertical elevation at different location x can be written as in Eq. (1). Here the phase angle ϕ is a random number uniformly distributed between 0 and 2π .

$$\eta_v = \eta_0 \cos(\omega t - kx - \phi) \quad (1)$$

Similarly, a surface wave particle's horizontal displacement can be written as in Eq.(2).

$$\eta_h = \eta_0 \sin(\omega t - kx - \phi) \quad (2)$$

The motion of a body can be calculated with its associated RAOs functions. For two bodies, i.e., the glacial ice feature and the structure, without losing generality, we can define the original location of the structure at $x=0$, and the location for the ice feature at $x = -(L^{ps} + L^{pi})$, see Figure 2 for the interpretation of symbols. We can select two reference points P_i and P_s on the ice feature and on the structure, respectively. It is mainly their relative motions that are of interest in deriving the impact heights and velocities. Figure 2 illustrates one of the many possible definitions of the reference points and their relative motion in a long wave with crest right at the $x=0$ point of the coordinate system. For this choice of reference points, when there is no wave, P_i and P_s coincide with each other at Still Water Level (SWL). With the above definitions and available RAOs, the heave motion of point P_s with reference to the centre of the platform's water plane at SWL is written in Eq. (3),

$$\eta_3^{ps} = \left| H_3^{ps}(\omega) \right| \eta_0 \cos(\omega t - kx - \phi) + L^{ps} \left| H_5^{ps}(\omega) \right| \eta_0 \cos(\omega t - kx - \phi) \quad (3)$$

in which, L^{ps} is the 'arm length' of the reference point P_s ; and the roll motion induced vertical motion is taken into account by multiplying this arm length by the roll displacement (angle) $\left| H_5^{ps}(\omega) \right| \eta_0 \cos(\omega t - kx - \phi)$. Similarly, point P_i 's heave motion with reference to the centre of

the ice feature's water plane at SWL is written in Eq. (4).

$$\eta_3^{pi} = \left| H_3^{pi}(\omega) \right| \eta_0 \cos(\omega t - kx - \phi) + L^{pi} \left| H_5^{pi}(\omega) \right| \eta_0 \cos(\omega t - kx - \phi) \quad (4)$$

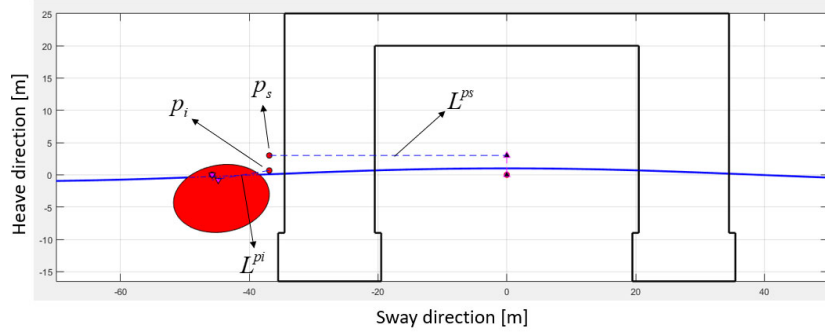


Figure 2. Definitions of symbols and the relative motion (sway and heave) between the ice feature (red) and structure (dark frames) in a relatively long wave component (blue line).

The relative vertical displacement among the two bodies can be written as in Eq. (5).

$$\Delta \eta_3 = \eta_3^{ps} - \eta_3^{pi} \quad (5)$$

For a floating body's sway displacement, one needs to use the water particle's horizontal motion (Eq. (2)) as the excitation together with the RAOs in the sway direction, i.e., $H_2(\omega)$. Generally, the sway displacement of a floating body can be written in Eq. (6), whose one time derivative leads to the sway velocity in Eq. (7).

$$\eta_2 = \left| H_2(\omega) \right| \eta_0 \sin(\omega t - kx - \phi) \quad (6)$$

$$\dot{\eta}_2 = \omega \left| H_2(\omega) \right| \eta_0 \cos(\omega t - kx - \phi) \quad (7)$$

Eq. (7) shows that the sway velocity is in phase with the heave motion of wave in Eq. (1), i.e. the maximum sway velocity is attained when the heave motion is maximum.

The sway velocity for the structure and ice feature are written in Eqs. (8) and (9), respectively. For simplicity the roll motion's contribution to the sway velocity at the reference point is excluded, and at the same time not sacrificing too much accuracy.

$$\dot{\eta}_2^{ps} = \omega \left| H_2^{ps}(\omega) \right| \eta_0 \cos(\omega t - kx - \phi) \quad (8)$$

$$\dot{\eta}_2^{pi} = \omega \left| H_2^{pi}(\omega) \right| \eta_0 \cos(\omega t - kx - \phi) \quad (9)$$

The relative velocity between the ice feature and the structure is given by Eq.(10):

$$\Delta \dot{\eta}_2 = \dot{\eta}_2^{pi} - \dot{\eta}_2^{ps} \quad (10)$$

Relative motion in a sea state with random waves

For exemplifying purpose, we choose the same JONSWAP wave spectrum (see Figure 3) with reference to Block A at the 23rd licensing round in the Northern Barents Sea as a case study (Eik and Dezecot, 2016). The wave spectrum can be randomly seeded as a collection of bins with different width. Figure 3 illustrates one of such bins with a wave frequency of ω_i and

spectrum $S(\omega_i)$ in a sea state characterised by a set of parameters (i.e., with a significant wave height of $H_s = 13.8$ m, wave period $T_p = 18$ s, and with a 100-year return period $q = 10^{-2}$).

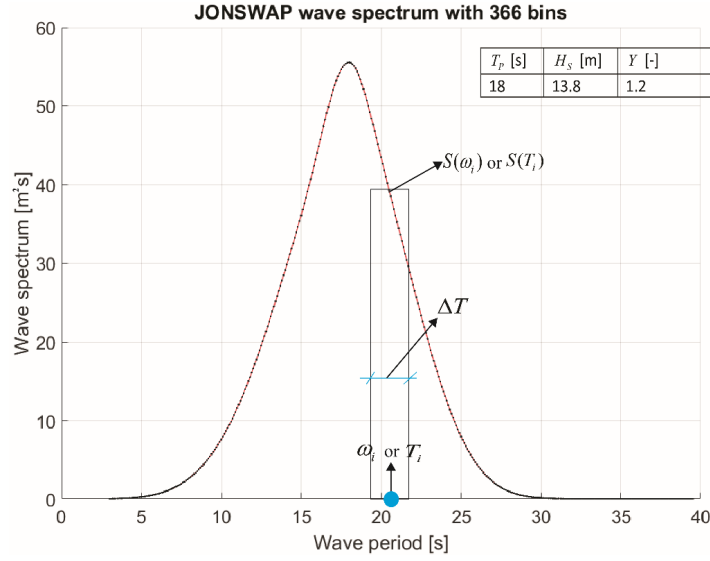


Figure 3. Selected sea state with an exaggerated bin width for definition of symbols.

Given the responses (re-written in Eq. (11)) from each single wave component ω_i with a wave height of η_i , one can write the overall response in Eq. (12).

$$\begin{aligned}
 \text{Relative heave displacement (rel-heave disp)} &\rightarrow \Delta \eta_{i,3}(\eta_i, \omega_i) = \eta_{i,3}^{ps}(\eta_i, \omega_i) - \eta_{i,3}^{pi}(\eta_i, \omega_i) \\
 \text{Relative sway velocity (rel-sway vel)} &\rightarrow \Delta \dot{\eta}_{i,2}(\eta_i, \omega_i) = \dot{\eta}_{i,2}^{pi}(\eta_i, \omega_i) - \dot{\eta}_{i,2}^{ps}(\eta_i, \omega_i) \\
 \text{Individual wave height for wave component } i \text{ with angular frequency } \omega_i \text{ is given } &\rightarrow
 \end{aligned} \tag{11}$$

$$\eta_i = \sqrt{2S(\omega_i) \cdot \Delta\omega} = \sqrt{2S(T_i) \cdot \frac{2\pi}{T_i^2} \cdot \Delta T}$$

$$\text{rel-heave disp } \Delta \eta_{Total,3} = \sum_{i=1}^N \Delta \eta_{i,3} \quad (N \text{ is the number of bins in Figure 3}) \tag{12}$$

$$\text{rel-sway vel } \Delta \dot{\eta}_{Total,2} = \sum_{i=1}^N \Delta \dot{\eta}_{i,2} \quad (N \text{ is the number of bins in Figure 3})$$

After the summation in Eq. (12), one also obtains the total relative heave displacement $\Delta \eta_{Total,3}(t)$ and total relative sway velocity $\Delta \dot{\eta}_{Total,2}(t)$. These two values offer us the correlated impact height and impact velocity's histories.

Sampling of impact events

After obtaining the relative motions in the time domain, one needs to sample impact events for further statistical analysis. Without losing generality, we consider here the impacts in the sway direction (see Figure 1), where the total relative heave displacement $\Delta \eta_{Total,3}(t)$ and total relative sway velocity $\Delta \dot{\eta}_{Total,2}(t)$ matter. Similar method can be applied to consider the impact in the vertical direction (e.g., impact with the pontoon of the semi-submersible).

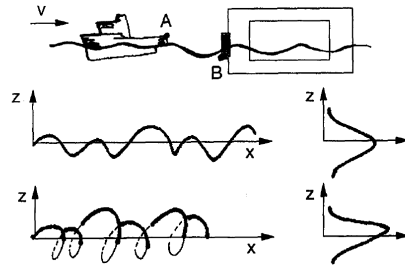


Figure 4. For ship and installation impacts (upper plot): sampling of impact events at high current velocity (middle plot) and low current velocity (lower plot), from Fylling (1994).

For this purpose, we adopt the same method that was introduced by Fylling (1994) for the analysis of ship impacts. When impacts in the horizontal direction (or sway direction under this paper's context) is considered, it is necessary to include current velocity to ensure that the ice feature drifts towards the structure. The drifting ship's impact scenario described by Fylling (1994) is illustrated in Figure 4. The ship (Body A) colliding with a structure (Body B) is under the influence of current with a velocity of V . With a high current velocity, the middle plot in Figure 4 shows the trajectory (heave in 'Z' and surge in 'X') of the ship; and each point on this trajectory is a potential and valid impact event. However, with a lower current velocity in the lower plot in Figure 4, the trajectory of the ship is moving back and forth. In this scenario, only the advancing surge motions are sampled as valid impact events (bold black line); whereas the negative surge motions (in thin black line) and the shielded positive surge motions (in dashed black line) are not considered as valid impact events. The sampling in both cases should be conducted with equal spacing in the surge direction, as when the ship approaches the structure, each point along the valid impact events trajectory (bold dark line) has an equal chance of impact. Using his sampling method, the impact events tend to skew towards to higher locations and larger velocities (e.g., see lower plot in Figure 4) when the current velocity is slow.

In summary, Fylling (1994) proposed two conditions to sample valid impact events out of the simulated bodies' motions. These are: 1) there is a positive impact velocity between the two bodies; and 2) only the non-shielded motion track has the chance of impact in the space domain. i.e., at the same point in the fixed space, there can only be one impact event.

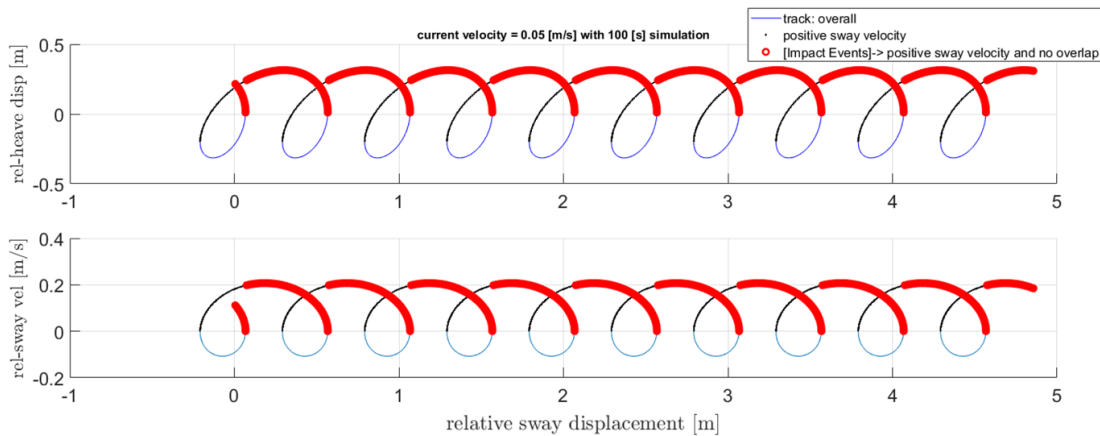


Figure 5. 100 second simulation with coupled motion track and sampled impact events under a slow current velocity = 0.05 m/s.

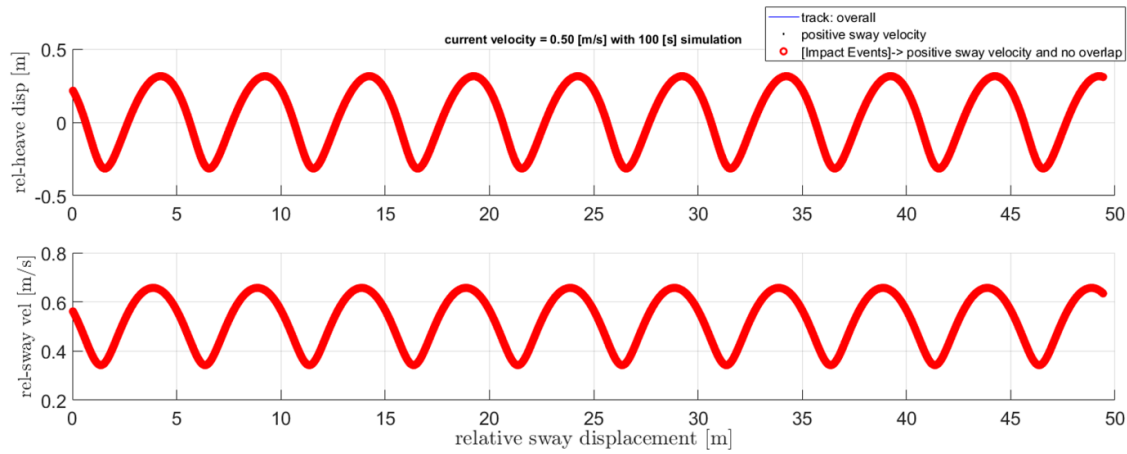


Figure 6. 100 second simulation with coupled motion track and sampled impact events under a faster current velocity = 0.5 m/s.

This method is implemented within MATLAB. With the formulation from Eq. (12), we first demonstrate this method with a single harmonic wave component under the influence of different current velocities. Given the coordinate system definition in Figure 1 and problem definition in Figure 2, the coupled motion tracks of the two impact bodies are shown in Figure 5 and Figure 6 for slow and fast current velocity scenarios. With this simple example, we see from the sampled impact events (i.e., red markers) that when the current velocity is slow, there exist a significant amount of shielding effect and most impact events are thereby skewing towards higher locations. This corresponds well with the conceptual plot in Figure 4 by Fylling (1994).

RESULTS AND DISCUSSIONS

The previous section laid the methods that can be utilised to construction two bodies' relative motions in a given sea state. Given the relative motion histories, impact events are sampled with the Fylling method (1994) equally in the spatial domain (in our case, in the sway direction). Applying this proposed method, the results of the case study (see Figure 2) are presented herein.

Relative motions

First, the relative motions characterised by Eq. (12) are presented herein. Because we have utilised the existing RAOs for each body from a previous study (Ekeberg et al., 2018), it is interesting to first compare the previous studies' frequency domain results to our time-domain simulated relative motion results (need to be converted into the frequency domain). The comparison in the frequency domain (RAOs, i.e., relative displacement (or velocity) over wave height) for the coupled heave and sway motions are presented in Figure 7 and Figure 8 respectively. The comparisons show little difference regarding the relative RAOs for both approaches. Only small discrepancies exist at several different wave frequencies locations. These might due to an inaccurate manual digitalisation of the existing RAOs for each body, based on which, the time domain analysis (i.e., Eqs. (1) to (12)) was carried out. In its totality, the favourable agreement of the two different approaches signifies the correctness of our new method. The advantage of the new method is that the relative motion track of the two bodies and thereby the correlated impact heights (quantified by $\Delta\eta_{Total,3}$) and velocities (quantified by

$\Delta\dot{\eta}_{Total,2}$) are direct outcomes.

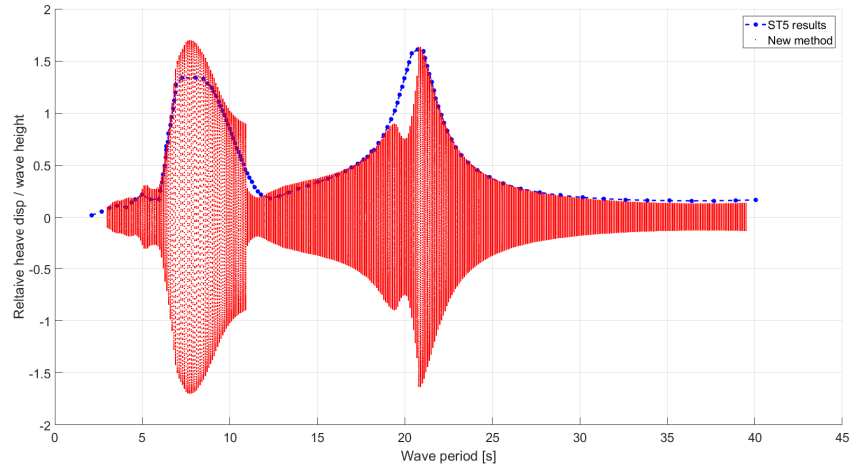


Figure 7: Relative heave displacement: time domain simulated results for each wave component (i.e., New method) comparing to previous frequency-domain results.

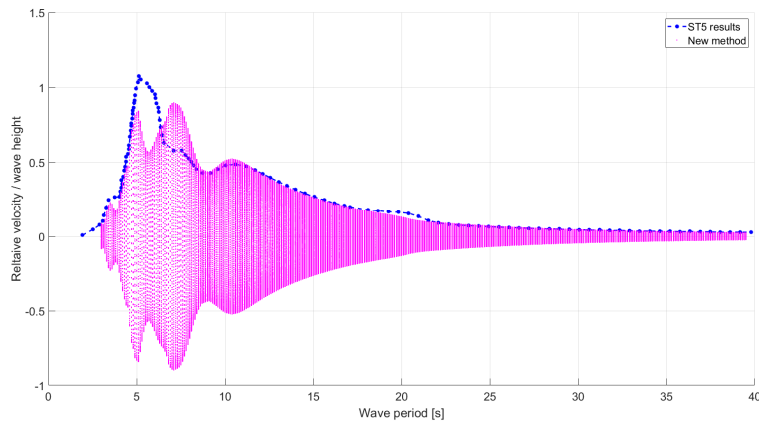


Figure 8: Relative sway velocity: time domain simulated results for each wave component (i.e., New method) comparing to previous frequency-domain results.

Impact events

To sample the impact events, the current influence should be included (as previously described). A current velocity of 0.79 m/s (from the physical environmental study by Eik and Dezcot (2016)) with a 100-year return period is selected as the base number for sampling the impact events from the simulated coupled motion histories. First, out of around 2×10^7 simulated motion tracks, given the current velocity of 0.79 m/s, around 1.2×10^7 motion events are sampled with positive velocity and non-shielded criteria., $\Delta\eta_{Total,3}$ versus $\Delta\dot{\eta}_{Total,2}$. However, the impact event at each location in the sway direction's trajectory has the same chance of impact. Impact events should be re-sampled in the spatial domain with equal sway displacement spacing in between. This is achieved via interpolation with a set of pre-defined equally spaced points in the sway displacement's direction to obtain their corresponding $\Delta\eta_{Total,3}$ versus $\Delta\dot{\eta}_{Total,2}$. In this regard, 1000000 impact events (green points) are further sampled in Figure 9.

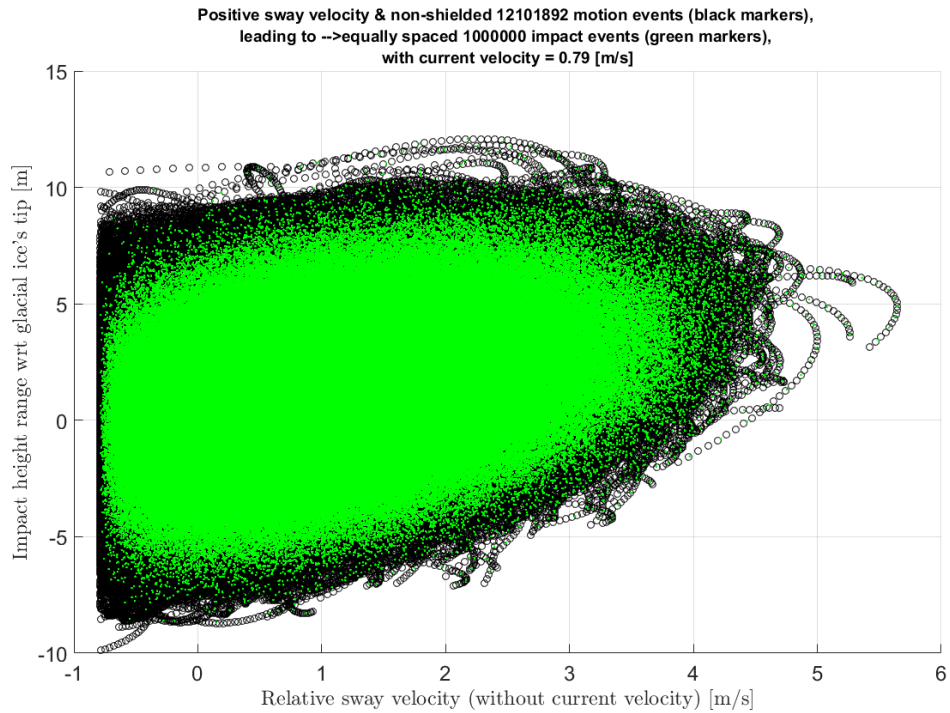


Figure 9: Impact events sampling: equally spaced impact events (green points) resampling.

These impact events contain correlated information of impact heights and velocities (i.e., $\Delta\eta_{Total,3}$ versus $\Delta\dot{\eta}_{Total,2}$), which will be the basis for the statistical analysis for the horizontal direction impact.

Impacts height and velocities

Impact heights' distribution

Given the impact events sampled in Figure 9, the impact height's probability distribution together with the best-fit function are presented in Figure 10 and Table a. The best fit obtained is the Normal distribution with parameters listed in Figure 10.

Table a: All sampled impact heights' statistical values (Note, impact events are sampled under the influence of a 0.79 m/s current velocity), unit: [m].

Non-exceedance level	50%	90%	99%
Normal distribution	± 1.8	± 4.4	± 6.7

Sway direction impacts' velocity distribution

Similarly, for all the sampled impact events' sway velocity, its statistical distribution are presented in Figure 11 and Table b. The best fit function obtained is the Weibull distribution with parameters listed in Figure 11.

Table b: All sampled sway velocity values (Note, velocity values in this study contains an additional 0.79 m/s current velocity), unit: [m/s].

Non-exceedance level	50%	90%	99%
Weibull distribution	1.8	3.0	4.0

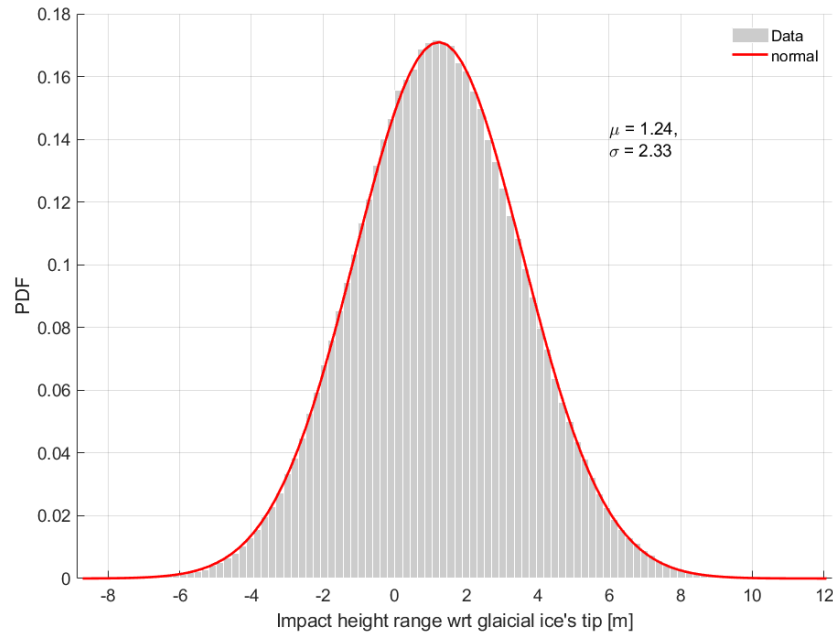


Figure 10: Statistical distribution of all sampled impact heights' values, unit: [m].

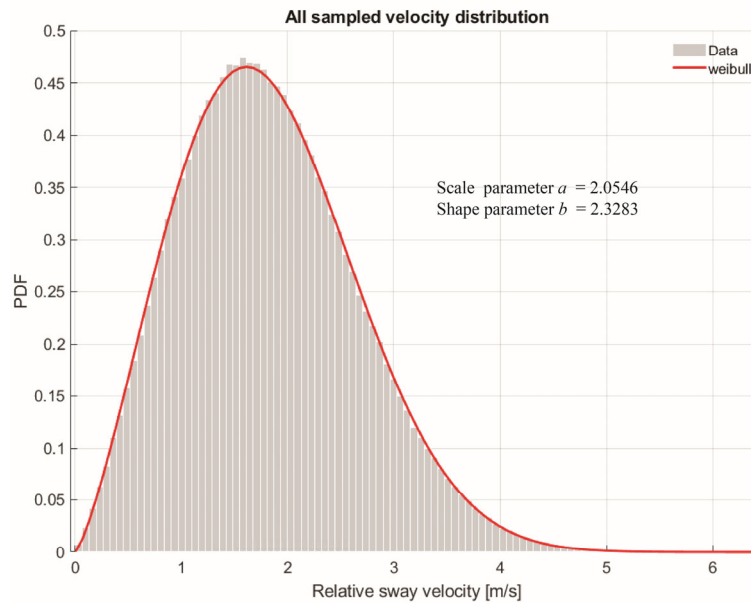


Figure 11: Statistical distribution of all sampled impact velocities in sway direction, unit: [m/s].

Given the sampled impact events, we can separate the impact height range with several bins. The forthcoming analyses include 6 different bins, whose centre are listed in Table c. Within each bin, a subset of impact velocities is available and the statistical analyses upon them were carried out. The best probabilistic fitting functions together with the parameters within different bins are summarised in Table c. The Weibull distribution gives the best fit for most of the bins, whereas the Nakagami and Generalized extreme value distribution fit best at the two ends of the height direction. One explanation to the inconsistent best-fit functions at the upper and lower end of the impact height direction could be that at these two ends (i.e., extremely high and extremely low impact locations), relatively smaller amount of simulated impact events are available to obtain the consistent Weibull distribution as appeared for other bins.

Table c: Sampled sway velocity values' statistic distribution within different bins at different impact height range (Note, velocity values in this study contain an additional 0.79 m/s current velocity), unit: [m/s].

Centre of bins [m]	Best fit distributions	Best fit parameters
-6.9825	Nakagami	$m = 1.0487$ $\Omega = 1.5175$
-3.5175	Weibull	$\lambda = 1.5791$ $k = 2.1874$
-0.0526	Weibull	$\lambda = 1.9127$ $k = 2.3359$
3.4123	Weibull	$\lambda = 2.2696$ $k = 2.5768$
6.8773	Weibull	$\lambda = 2.7021$ $k = 2.8947$
10.3422	Generalized extreme value	$\mu = -0.3101$ $\sigma = 0.8876$ $\xi = 2.6074$

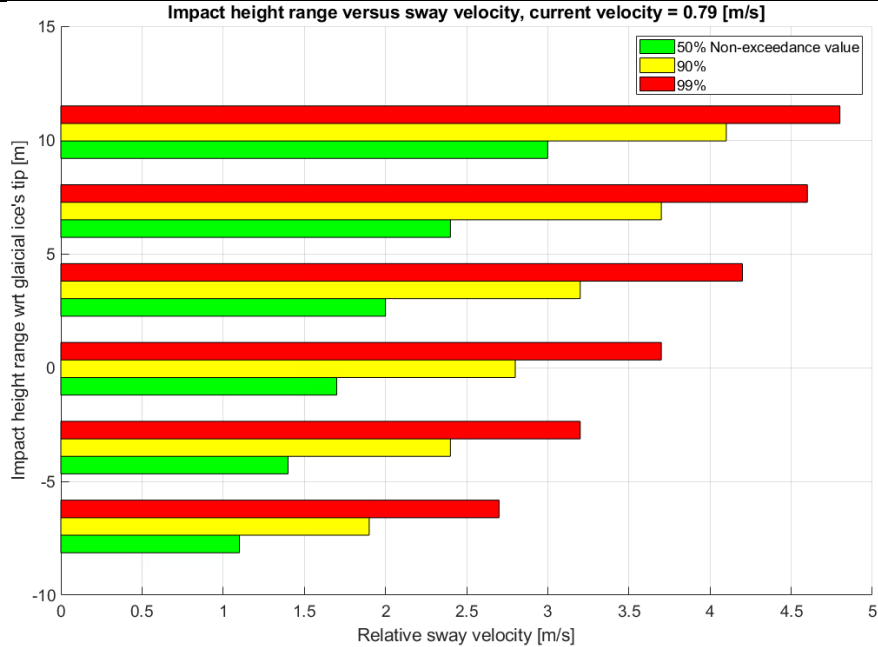


Figure 12: Impact velocities in sway direction at different heights with different non-exceedance levels.

With the best-fit functions, we can derive the 50%, 90% and 99% non-exceedance relative sway velocities at different bins (at different heights). This is visualised in Figure 12. To further put the calculated results into context, the same impact velocities' distribution together with its associated impact probability are plotted in Figure 13 with reference to the position and geometries of the structure. It is noticed that the impacts velocity is large at the high locations, but the probability of impact is small. As expected, the impacts reactions are skewed towards higher elevations given the selected current velocity, 0.79 m/s.

CONCLUSIONS

This paper focuses on deriving the correlated impact velocities and heights with a linear wave theory-based body motion simulation and an impact events sampling method. To demonstrate the method, we performed a case study showing the impact between an ellipsoidal glacial ice feature and a semi-submersible structure. Focuses was placed on the horizontal impact scenario as a two-dimensional problem. The proposed method manages to construct tens of millions of impact events, out of which, the statistical distribution of horizontal impact velocities in the height direction is obtained. This information is critical to perform related local damage assessment in the followed-up studies. Based on the case study under the given sea state, the

following observations are made through the analysis.

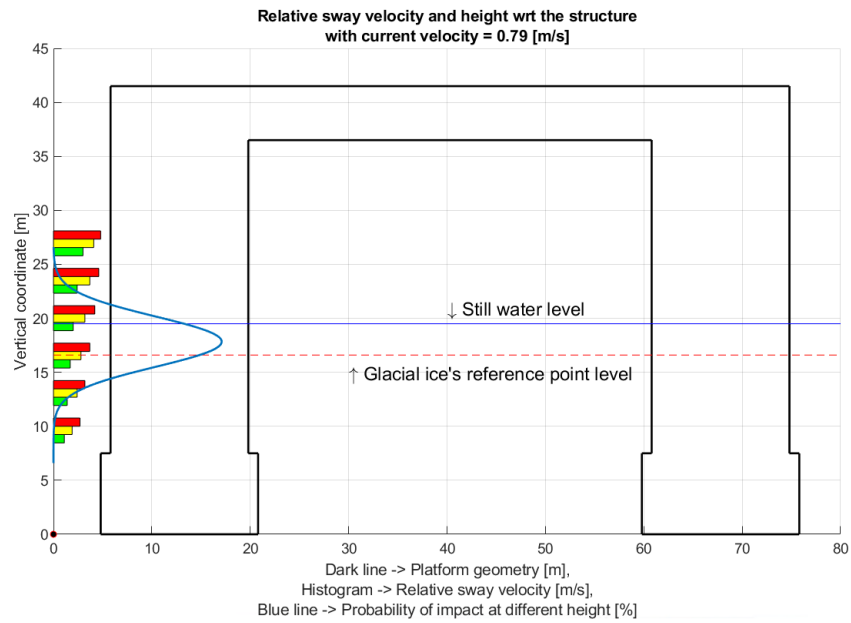


Figure 13: Impact velocities in sway direction and the associated impact probability at different heights with reference to the structure.

- The horizontal impact velocities increase with the impact height (see Figure 12).
- The most probable horizontal impact with the ice tip occurs around the SWL (e.g., the maximum probability of impact in Figure 13).
- There is a rather low chance to have a horizontal impact either with the pontoon (12.5 m below SWL) or with anywhere say, 5 m above SWL (see Figure 13).
- The presence of current velocity is shown to influence the sampling process and thereby influencing the impact velocity's distribution. Lower current velocity introduces a higher amount of 'shielding' effect and the impact velocity distribution tends to skew towards higher impact locations.
- The proposed method is rather effective in construction a large amount of potential impact events (i.e., in the order of millions) from which, sensible distributions of impact information can be obtained.

ACKNOWLEDGEMENTS

The authors would like to thank the financial sponsorship from the Petroleum Safety Authority Norway (Ptil: Petroleumstilsynet) to carry out this study. The first author would also like to thank VISTA – a basic research program in collaboration between The Norwegian Academy of Science and Letters, and Equinor (former Statoil), for financial support in writing this paper.

REFERENCES

- EIK, K. J. & DEZECOT, C. 2016. Barents Sea exploration collaboration, "Fysisk miljø i Barentshavet sørøst,".
- EKEBERG, O.-C., SHIPILOVA, O., BIRKNES-BERG, J. & JOHANSEN, A. 2018. Glacial Ice Impact. FYLLING, I. On the Statistics of Impact Velocities and Hit Positions Related to Collisions and Mating Operations for Offshore Structures. BOSS, 1994. 297-306.